

## FIELD COMPUTATIONS BY THE COMPLEMENTARY NETWORKS

Y. Saito, S. Hayano and N. Tsuya

**Abstract** - The method of magnetic circuits has been proposed for evaluating the 3-D magnetodynamic fields in electromagnetic devices [1-3]. In this paper, we elucidate that our previous magnetic circuit method is one of the complementary network methods. Since the complementary network method is fundamentally based on the geometrical dual property associated with the element discretizations, it is found that this method is quite useful to give a circuit interpretation of field computations [4]. As an illustrative example, the dynamic fields in a toroidal reactor are computed by the complementary network method.

## INTRODUCTION

In order to implement the finite element method in the most efficient manner, Penman and others have proposed the dual finite element method based on the inherent property in vector fields [5]. The conventional first order triangular finite element method is one of the primal energy methods, and has been given a circuit interpretation by Carpenter [4]. The successful magnetic field calculations have been previously carried out by the circuit representation method, which has not been based on any energy methods but one of the finite difference methods [1-3].

In this paper, we elucidate that our previous circuit method is one of the complementary energy methods. Our complementary energy method proposed in this paper is fundamentally based on the geometrical dual property associated with the discretizations so that the implementation of complementary energy method proposed by Penman and others has to use the two types of potentials but our complementary energy method necessitates only one common potential for both primal and complementary functionals. Furthermore, our method is quite useful to give a circuit interpretation of the field calculation schemes.

As an illustrative example, the dynamic fields in a toroidal reactor are computed by the complementary network method.

## BASIC EQUATIONS

The equations governing the electrodynamic fields are

$$\nabla \times E = - \partial B / \partial t, \quad (1)$$

$$\nabla \times H = J, \quad (2)$$

where  $E, J, B, H$  are respectively the electric field intensity, current density, magnetic flux density and magnetic field intensity. The electric field intensity  $E$  is related to the current density  $J$  as

$$E = \sigma J, \quad (3)$$

where  $\sigma$  is the resistivity of material. Furthermore, an auxiliary relationship between the magnetic flux density  $B$  and field intensity  $H$  is given by

$$H = (1/\mu)B + (1/s)(\partial B / \partial t), \quad (4)$$

where  $\mu, s$  are respectively the permeability and hysteresis coefficient of materials [3,6].

By means of (1)-(3), it is possible to derive a

The authors are with College of Engineering, Hosei University, 3-7-2 Kajinocho Koganei, Tokyo 184, Japan.

following diffusion equation:

$$\sigma \nabla^2 H = \partial B / \partial t, \quad (5)$$

Generally, the leakage fluxes from iron core in a toroidal reactor are so small that most fluxes in a toroidal reactor may be regarded to flow through an iron core. This means that the magnetic flux density  $B$  and field intensity  $H$  in (5) are composed of their z-components as shown in Fig. 1(a). Thus (5) is reduced to

$$\sigma (\partial^2 H / \partial x^2) + \sigma (\partial^2 H / \partial y^2) = \partial B / \partial t, \quad (6)$$

for a cross section of toroidal reactor.

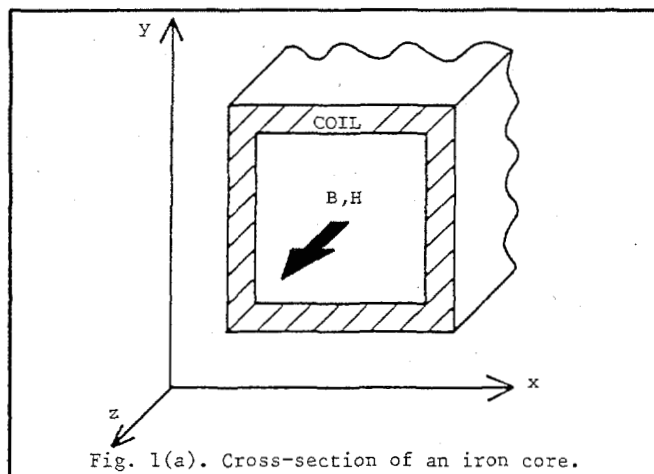


Fig. 1(a). Cross-section of an iron core.

## THE COMPLEMENTARY NETWORK THEORY

## Local one dimensional method

When the problem region is subdivided into the triangular finite elements shown in Fig. 1(b), then the lines connected the vertices  $i, j$  and the centers 1, 2 of outer circle are always perpendicularly intersecting each other. Thereby, two independent trial

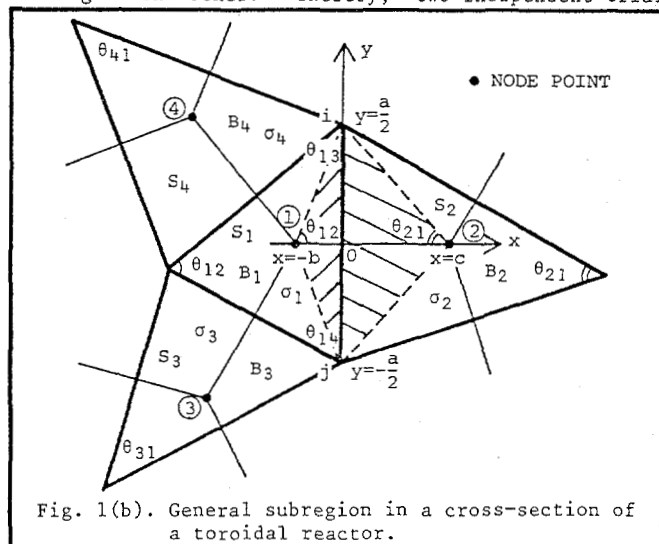


Fig. 1(b). General subregion in a cross-section of a toroidal reactor.

functions are possible; one takes the vertices 1, j as the node points; and the other takes the centers 1, 2 of outer circle as the node points. In the other words, on the local x-y coordinate system shown in Fig. 1(b), it is possible to assume that (5) is divided into the following two parts:

$$\sigma(\partial^2 H/\partial y^2) = (1/2)(\partial B/\partial t), \quad (7)$$

$$\sigma(\partial^2 H/\partial x^2) = (1/2)(\partial B/\partial t). \quad (8)$$

In most cases, one of the equations (7) and (8) is sufficient to represent the magnetic fields, therefore, it may be possible to assume that whole field in Fig. 1(a) consists of the solutions obtained by the local one dimensional equation (8). One of the methods based on (7) is a first order triangular finite element method whose node points coincide with the vertices of principal triangles.

#### Functional and boundness

The nodes 1, 2 are located on the x-axis in Fig. 1(b). This means that the rate of change  $\sigma(\partial H/\partial x)$  must be continuous from the regions 1 to 2 in Fig. 1(b). Thereby, a complementary functional  $G(H)$  is given by

$$G(H) = -\int (1/\sigma)(\sigma \partial H/\partial x)^2 dx dy + \int \hat{H}(\partial B/\partial t) dx dy, \quad (9)$$

where  $\hat{H}$  denotes the value of magnetic field intensity at node points, and the integrations are carried out over the hatched regions 1, 2 in Fig. 1(b).

To show that the functional  $G(H)$  in (9) reaches to a maximum at true solution of (8), let  $H$  denote the true solution of (8), and  $\varphi$  is some differentiable function which takes non-zero value in the regions 1, 2 in Fig. 1(b) but vanishes at all prescribed boundaries, then the approximate functional  $G(H+\epsilon\varphi)$  is written by

$$G(H+\epsilon\varphi) = G(H) - \epsilon \int [2\sigma(\partial H/\partial x)(\partial\varphi/\partial x) + \varphi(\partial B/\partial t)] dx dy - \epsilon^2 \int \sigma(\partial\varphi/\partial x)^2 dx dy, \quad (10)$$

where  $\epsilon$  is a numerical parameter. Extremization of (10) yields

$$\begin{aligned} \delta G &= \lim_{\epsilon \rightarrow 0} [G(H+\epsilon\varphi) - G(H)]/\epsilon \\ &= -\int [2\sigma(\partial H/\partial x)(\partial\varphi/\partial x) + \varphi(\partial B/\partial t)] dx dy \\ &= -\int 2\sigma\varphi(\partial H/\partial x) dy + \int \varphi [2\sigma(\partial^2 H/\partial x^2) - \partial B/\partial t] dx dy \\ &= 0. \end{aligned} \quad (11)$$

By means of (11), it is revealed that an extremization of (10) enforces the second term on the right of (10) to be zero and reaches to the true solution of (8). The third term on the right of (10) is always negative value so that the approximate functional  $G(H+\epsilon\varphi)$  is always smaller than the true functional  $G(H)$ , that is

$$G(H+\epsilon\varphi) \leq G(H). \quad (12)$$

In the other words, a maximum will be reached when  $\epsilon$  has zero value.

#### Node equations

The complementary functional  $G(H)$  in (9) has been derived by preconditioning a following relation:

$$\sigma_1 \left. \left( \frac{\partial H}{\partial x} \right) \right|_{\text{REGION 1}} = \sigma_2 \left. \left( \frac{\partial H}{\partial x} \right) \right|_{\text{REGION 2}}, \quad (13)$$

where  $\sigma_1, \sigma_2$  are respectively the resistivities of the regions 1 and 2 in Fig. 1(b). According to (2) and (3), (13) means that the electric field intensities in a y-direction at the boundary must be common to both regions 1 and 2 in Fig. 1(b). Furthermore, it is obvious that the first and second terms on the right of (9) are corresponding to the dissipative and input powers, respectively.

In order to derive the trial functions which satisfy the condition (13), let  $H_0$  denote the magnetic field intensity at the origin  $O$  of local coordinate system shown in Fig. 1(b), then the trial functions  $H_a$  and  $H_b$  for the regions 1 and 2 are respectively assumed to

$$H_a = H_0 + (H_0 - H_1)(x/b), \quad (14)$$

$$H_b = H_0 + (H_2 - H_0)(x/c), \quad (15)$$

where  $H_1$  and  $H_2$  are respectively the field intensities of the node points 1 and 2; and the lengths  $b, c$  are shown in Fig. 1(b). Substitution (14) and (15) into (13) yields

$$(H_0 - H_1)(\sigma_1/b) = (H_2 - H_0)(\sigma_2/c) \quad (16)$$

or

$$H_0 = [(\sigma_1/b)H_1 + (\sigma_2/c)H_2] / [(\sigma_1/b) + (\sigma_2/c)]. \quad (17)$$

By means of (17), (14) and (15) are respectively reduced to

$$H_a = [(\sigma_1/b)H_1 + (\sigma_2/c)H_2] / [(\sigma_1/b) + (\sigma_2/c)] + (H_2 - H_1)(\sigma_2/bc)x / [(\sigma_1/b) + (\sigma_2/c)], \quad (18)$$

$$H_b = [(\sigma_1/b)H_1 + (\sigma_2/c)H_2] / [(\sigma_1/b) + (\sigma_2/c)] + (H_2 - H_1)(\sigma_1/bc)x / [(\sigma_1/b) + (\sigma_2/c)]. \quad (19)$$

By introducing (18) and (19) into (9), a functional  $G(H_a, H_b)$  becomes to

$$G(H_a, H_b) = -(1/2)(H_2 - H_1)^2 / [(b/a\sigma_1) + (c/a\sigma_2)] - (ab/2)H_1(\partial B_1/\partial t) - (ac/2)H_2(\partial B_2/\partial t), \quad (20)$$

where  $B_1, B_2$  are respectively the flux densities in the regions 1 and 2; also the length  $a$  is shown in Fig. 1(b).

Maximizing (20) gives the following node equations:

$$\begin{aligned} \partial G(H_a, H_b) / \partial H_1 &= (H_2 - H_1) / [(b/a\sigma_1) + (c/a\sigma_2)] \\ &\quad - (ab/2)(\partial B_1/\partial t) = 0, \end{aligned} \quad (21)$$

$$\begin{aligned} \partial G(H_a, H_b) / \partial H_2 &= (H_1 - H_2) / [(b/a\sigma_1) + (c/a\sigma_2)] \\ &\quad - (ac/2)(\partial B_2/\partial t) = 0, \end{aligned} \quad (22)$$

(21) and (22) are respectively corresponding to the nodes 1 and 2 in Fig. 1(b). The node equations of the other regions can be obtained in much the same way as (21). Hence, a equation for the node 1 in Fig. 1(b) can be obtained as

$$\sum_{k=2}^4 [(H_k - H_1) / \langle (1/2\sigma_1 \tan\theta_{1k}) + (1/2\sigma_k \tan\theta_{k1}) \rangle] - S_1 (\partial B_1 / \partial t) = 0, \quad (23)$$

where the angles  $\theta_{1k}$ ,  $\theta_{k1}$  and area  $S_1$  are shown in Fig. 1(b).

Complementary networks

To derive a network model, let  $\Delta z$  denote the length of iron core in a z-direction of Fig. 1(a), then (23) is modified to

$$\sum_{k=2}^4 [(i_k - i_1) / \langle (1/R_{1k}) + (1/R_{k1}) \rangle] - (\partial \phi_1 / \partial t) = 0, \quad (24)$$

where the currents  $i_k$ , flux  $\phi_1$  and electric resistances  $R_{1k}$ ,  $R_{k1}$  are

$$\left. \begin{aligned} i_k &= \Delta z H_k, \quad k=1,2, \dots, 4 \\ \phi_1 &= S_1 B_1, \\ R_{1k} &= 2\sigma_1 \tan\theta_{1k} / \Delta z, \quad R_{k1} = 2\sigma_k \tan\theta_{k1} / \Delta z, \quad k=2,3,4 \end{aligned} \right\} \quad (25)$$

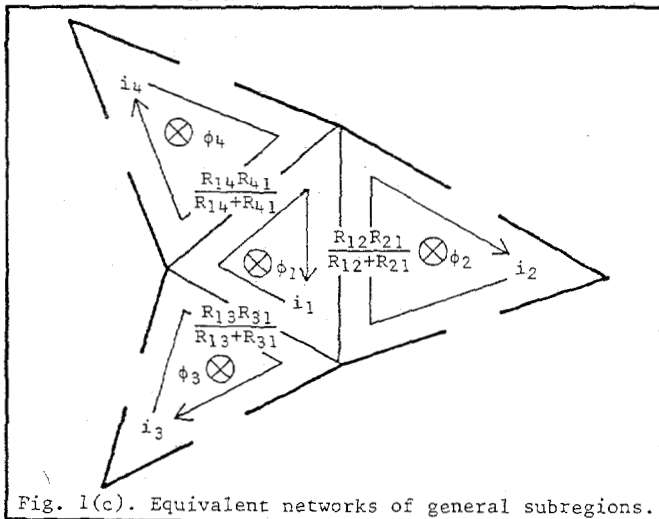
By means of (24), it is possible to depict a network model of Fig. 1(b) as shown in Fig. 1(c). In order to derive a network model of whole regions shown in Fig. 1(a), it is required to introduce an auxiliary relationship for an exciting coil region, and this is given by

$$R_e i_e + n (\partial / \partial t) \sum_{k=1}^m \phi_k = v, \quad (26)$$

where  $R_e, n, i_e, v$  are the electric resistance of coil, number of turns of coil, exciting current, impressed voltage;  $\phi_k$  ( $k=1,2, \dots, m$ ) are the fluxes; and  $m$  is the total number of node points, respectively. Furthermore, according to (2) and (4), the exciting current  $i_e$  and eddy currents  $i_k$  ( $k=1,2, \dots, m$ ) are related with the magnetic circuits as

$$\left. \begin{aligned} n i_e + i_k &= M_k \phi_k + N_k (\partial / \partial t) \phi_k, \\ k &= 1,2, \dots, m \end{aligned} \right\} \quad (27)$$

where  $\Delta z_k, S_k, \mu_k, s_k$  are respectively the length in a



z-direction, area, permeability, hysteresis coefficient of the subregion  $k$ ; and

$$M_k = \Delta z / \mu_k S_k, \quad N_k = \Delta z_k / s_k S_k. \quad (28)$$

By combining (24)-(28), it is possible to obtain the following system of equations:

$$RI + W(d/dt)\phi = V, \quad (29)$$

$$W^T I = M\phi + N(d/dt)\phi, \quad (30)$$

where a superscript T refers to the transposed matrix. The current vector  $I$  in (29), (30) consists of an exciting current  $i_e$  in (26) and eddy currents  $i_k$  ( $k=1, 2, \dots, m$ ), and is a column vector of order  $m+1$ . The voltage vector  $V$  in (29) consists of a source voltage  $v$  and the other elements have zero values, and is a column vector of order  $m+1$ . The flux vector  $\phi$  in (29), (30) consists of the fluxes  $\phi_k$  ( $k=1,2, \dots, m$ ), and is a column vector of order  $m$ . The resistance matrix  $R$  consists of the electrical resistance  $R_e$  in (26) and electric resistances of eddy current paths e.g.  $R_{1k}$  in (24), and is a square matrix of order  $m+1$ . The winding matrix  $W$  consists of the number of turns  $n$  in (26) and unit turn for eddy current paths, and is a rectangular matrix with  $m+1$  rows and  $m$  columns. The magnetic resistance matrix  $M$  in (30) consists of the magnetic resistances  $M_k$  ( $k=1,2, \dots, m$ ) in (28), and is a diagonal matrix of order  $m$ . Finally, the hysteresis parameter matrix  $N$  consists of the hysteresis parameters  $N_k$  ( $k=1,2, \dots, m$ ) in (28), and is a diagonal matrix of order  $m$ .

Thus, a consideration of (29) and (30) gives an equivalent circuit of the toroidal reactor as shown in Fig. 1(d).

Time discretization

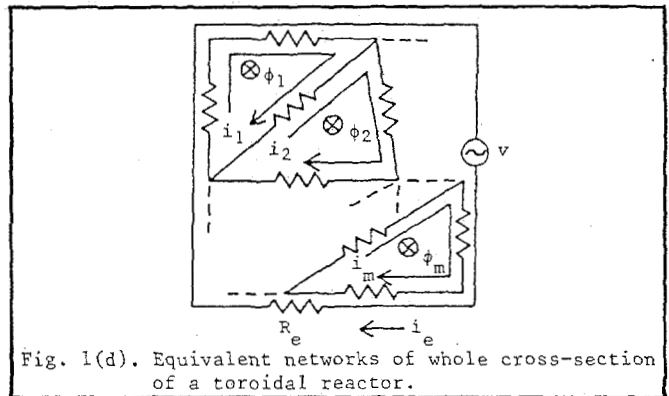
By means of (29) and (30), it is possible to write a system of equations as

$$W^T R^{-1} V = M\phi + (W^T R^{-1} W + N)(d/dt)\phi, \quad (31)$$

where a superscript  $-1$  refers to the inversed matrix. (31) is discretized in time  $t$  in the following way:

$$\begin{aligned} W^T R^{-1} V_{t+(\Delta t/2)} &= M_{t+(\Delta t/2)} (1/2) [\phi_{t+\Delta t} + \phi_t] \\ &+ [W^T R^{-1} W + N_{t+(\Delta t/2)}] (1/\Delta t) [\phi_{t+\Delta t} - \phi_t], \end{aligned} \quad (32)$$

where  $\Delta t$  is a stepwidth in time; and the subscripts  $t, t+\Delta t, t+(\Delta t/2)$  refer to the time  $t, t+\Delta t, t+(\Delta t/2)$ , respectively. It must be noted that the elements in magnetic resistance matrix  $M$  and hysteresis parameter



matrix  $N$  are generally nonlinear functions of flux and time derivative of flux, so these nonlinearities are taken into account in (32).

**Results**

Various constants used in the calculations are listed in Table 1, and the magnetization curves for the permeability  $\mu$  and hysteresis coefficient  $s$  are shown in [3].

For comparisons, (32) was iteratively solved in two typical cases. One is with solid core, and the other is with laminated core. As a result, it has been found that the eddy currents strongly dominate the dynamic fields in a solid core, but the nonlinear magnetization characteristics of material dominate the dynamic fields in a laminated core. Fig. 2(a) shows an example of transient fluxes in a solid core, also Fig. 2(b) shows the local fluxes in a solid core. Fig. 2(c) shows an example of the dynamic magnetizations in a laminated core.

**CONCLUSIONS**

As shown above, we have proposed a new method which is based on the complementary functional and geometrical dual property associated with the discretizations. The complementary network method makes the source term, e.g.  $\partial B/\partial t$  in (16), in each of the elements be independent to the other elements, and this gives an equivalent circuit which is well corresponding to the physical picture of fields. Our method has been exploited for designing the devices utilizing a new magnetic material [7].

Finally, the authors greatly appreciate to Mr. M. Matsueda for his programing and experimental works.

**REFERENCES**

- [1] Y. Saito, "Three dimensional analysis of nonlinear magnetodynamic fields in a toroidal reactor," *Comp. Meths. Appl. Mech. Eng.*, Vol. 22, No. 3, June 1980, pp. 289-308.
- [2] Y. Saito, "Theory of magnetic circuits for nonlinear magnetic fields in electromagnetic devices," *Procs. Second Inter. Sym. Inno. Nu. Ana. Appl. Eng. Scis.*, Montreal Québec, 1980, pp. 13-22.
- [3] Y. Saito, "Three dimensional analysis of magnetodynamic fields in electromagnetic devices taking into account the dynamic hysteresis loops," *IEEE Transactions on Magnetics*, Vol. MAG-18, No. 2, March 1982, pp. 546-551.
- [4] C. J. Carpenter, "Finite element network models and their application to eddy current problems," *Proc. IEE*, Vol. 122, No. 4, April 1975, pp. 455-462.
- [5] J. Penman, J. R. Fraser, "Complementary and dual finite element principles in magnetostatics," *IEEE Transactions on Magnetics*, Vol. MAG-18, No. 2, March 1982, pp. 319-324.
- [6] Y. Saito, S. Hayano, T. Yamamura and N. Tsuya, "A representation of magnetic hysteresis," *IEEE Transaction on Magnetics*, Vol. MAG-25, No. 5, September 1984, pp. 1434-1436.
- [7] K. I. Arai and N. Tsuya, "Ribon-form silicon-iron alloy contained 6.5 percent silicon," *IEEE Transactions on Magnetics*, Vol. MAG-16, No. 1, Janu. 1980, pp. 126-129.

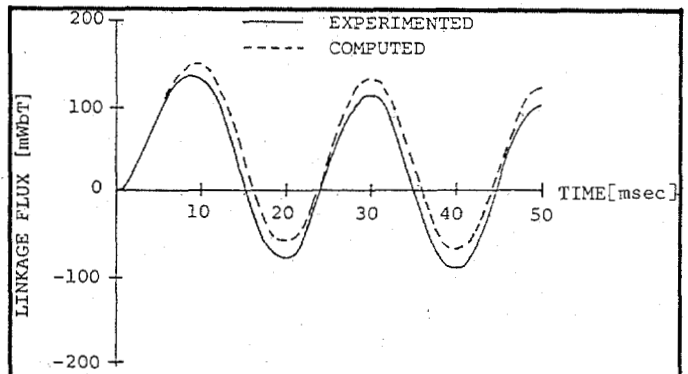


Fig. 2(a). Transient of total flux together with the experimented values in a solid core, where a start angle is 33.0 degree.

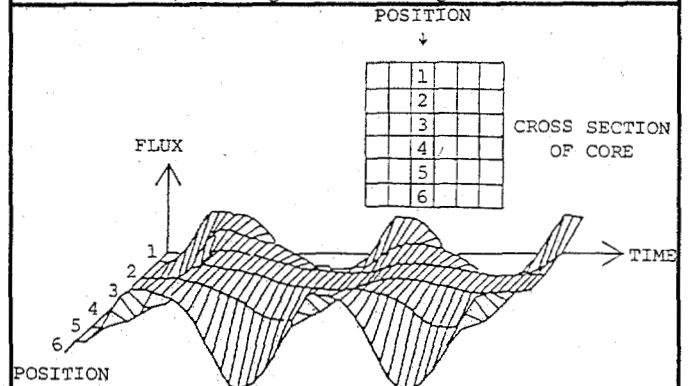


Fig. 2(b). Transient of local fluxes in a solid core, where a start angle is 33.0 degree.

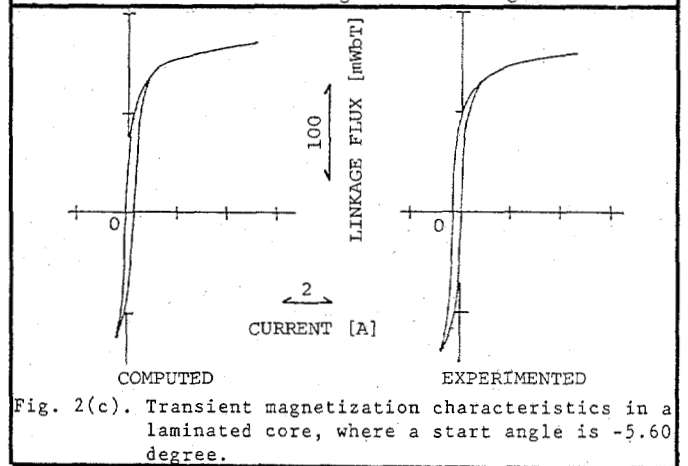


Fig. 2(c). Transient magnetization characteristics in a laminated core, where a start angle is -5.60 degree.

Table 1. Various constants used in the calculations.

Number of node points (72 right-angled isosceles triangles)	$m = 36$
Number of turns of coil	$n = 900$
Outer radius of core	0.05 [m]
Inner radius of core	0.04 [m]
Cross-sectional area of core	0.0001 [m <sup>2</sup> ]
Resistance of coil- Solid core	$R_s = 6.52[\Omega]$
- Laminated core	$R_e = 6.23[\Omega]$
Resistivity of core- Solid core	$\sigma = 20.6 [\mu\Omega\text{cm}]$
- Laminated core	$\sigma = \infty [\Omega\text{m}]$
Source voltage (sinusoidal wave)	$v = 30$ [V]
Frequency	$f = 50$ [Hz]
Stepwidth	$\Delta t = 0.2$ [msec]